

# Effect of the Porosity of a Polymer of Intrinsic Microporosity (PIM) on Its Intrinsic Fluorescence

Shaohua Chen,<sup>†,||</sup> Wei Yi,<sup>†</sup> Jean Duhamel,<sup>\*,†</sup> Kathleen Heinrich,<sup>‡,⊥</sup> Gisela Bengtson,<sup>‡</sup> and Detlev Fritsch<sup>\*,§</sup>

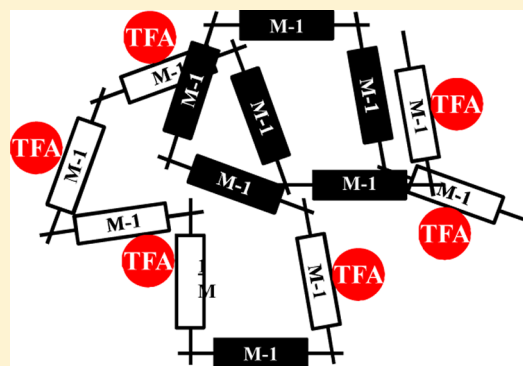
<sup>†</sup>Institute for Polymer Research, Waterloo Institute of Nanotechnology, Department of Chemistry, University of Waterloo, Waterloo, ON N2L 3G1, Canada

<sup>‡</sup>Helmholtz-Zentrum Geesthacht, Institut für Polymerforschung, Max-Planck-Strasse 1, 21502 Geesthacht, Germany

<sup>§</sup>Fraunhofer IAP, FB3, Geiselbergstrasse 69, 14476 Potsdam-Golm, Germany

## Supporting Information

**ABSTRACT:** The photophysical properties of a polymer of intrinsic microporosity, namely, PIM-1, were characterized by steady-state and time-resolved fluorescence for solutions of PIM-1 in dichloromethane (DCM) or for a membrane made of PIM-1 immersed in hexane to which a quencher was added. Quenching of PIM-1 by the proton-donor trifluoroacetic acid (TFA), electron-rich tributylamine (TBA), and electron-poor nitromethane ( $\text{CH}_3\text{NO}_2$ ) was investigated and compared to those of the structural unit of PIM-1, the model compound M-1. Only TBA and TFA appeared to quench PIM-1 effectively. The sensitivity of monomer M-1 to the nature of the solvent led us to investigate how addition of a quencher would affect the fluorescence of the polymer PIM-1. Solvent effects were observed for TFA only and were carefully characterized. In particular, it was determined that these solvent effects could be neglected for TFA concentrations smaller than 1.4 mM. Quenching of PIM-1 by TBA was diffusional in nature and occurred in a similar manner for M-1 and PIM-1 in DCM, suggesting that M-1 is locally excited in PIM-1. All M-1 units were accessible and quenched effectively by TBA for PIM-1 in DCM and the PIM-1 membrane in hexane. Quenching of PIM-1 in DCM and in the membrane was more complex, showing a combination of static, diffusive, and protective quenching. The fraction of accessible M-1 units to TFA ( $f_a$ ) was determined to be equal to 0.5 for PIM-1 in DCM or in the membrane. The TBA and TFA quenching experiments led to the conclusion that the same accessibility was obtained for the fluorescent constituting units of PIM-1 dissolved in DCM or in a membrane immersed in hexane, in agreement with the known high microporosity of this polymer.



## INTRODUCTION

Since their discovery in 2004,<sup>1</sup> polymers of intrinsic microporosity (PIMs)—a novel class of polymers with micropores smaller than 2 nm—have attracted great interest especially for their use in membranes.<sup>2–4</sup> PIMs belong to a class of polymers that can generate very large fractional free volumes (ffv's), typically with values greater than 20%. This property is a consequence of their polymeric backbones which are composed of highly rigid and contorted molecular elements which prevent their efficient packing. Astonishingly, PIMs can be synthesized by step-growth polymerization to high molecular weight, resulting in materials with good mechanical features forming flexible, free-standing films that consist of a network of interconnected molecular-sized pores yielding extraordinarily high surface areas.<sup>1–4</sup> PIMs have been used in a wide range of applications, to prepare membranes for gas separation or nanofiltration,<sup>5–9</sup> hydrogen storage,<sup>10</sup> sensor application,<sup>11,12</sup> and heterogeneous catalysis.<sup>4</sup>

To date, most studies on PIMs have focused on improving their synthesis,<sup>13</sup> introducing new rigid monomers into their backbone,<sup>14–18</sup> and, not surprisingly, considering the properties of PIMs, characterizing their inherent porosity.<sup>10,13,15,19–23</sup> The porosity of PIMs has been characterized in terms of their ffv and pore size using a variety of techniques such as sorption isotherms acquired with  $\text{N}_2$ , Xe, and a number of other gases,<sup>10,19–22</sup> positron annihilation lifetime spectroscopy (PALS),<sup>19,21,23,24</sup> or  $^{129}\text{Xe}$  NMR spectroscopy.<sup>19</sup> These studies have established that PIMs have surface areas between 450 and 1000  $\text{m}^2\text{g}^{-1}$  from  $\text{N}_2$ -sorption isotherms, pore diameters smaller than 2.0 nm, a feature that qualifies PIM membranes as being microporous, and ffv's between 20 and 30%. This high porosity is achieved by using building blocks for the polymer backbone that are rigid and possess a site of contortion (such as

Received: July 19, 2012

Revised: March 19, 2013

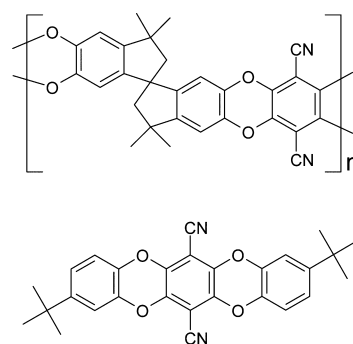
Published: March 21, 2013

a spiro-center) that prevent the efficient packing of the chains. Rigid blocks are typically aromatic molecules such as phthalocyanine<sup>22</sup> or triptycene.<sup>16</sup> In turn, incorporation of these aromatic molecules into PIMs together with two electron pulling cyano groups yields highly colored polymers that absorb and emit visible light.<sup>1,4</sup>

The well-established combination of high porosity and ability to fluoresce exhibited by PIMs led us to investigate whether fluorescence quenching experiments might provide complementary molecular information about the microstructure of PIMs and their interactions with different chemicals. Any quenching fluorescence experiment deals typically with a fluorescent macromolecule in solution.<sup>25</sup> The fluorophore used to probe the macromolecule can be intrinsic when it is a constituting unit of the macromolecule as for PIMs or extrinsic when it is covalently attached to the macromolecule. Upon addition of a quencher to the solution, the quencher will inhibit the emission of the fluorescent macromolecule if the intrinsic or extrinsic fluorophore is accessible to the solvent. In this case, a linear increase is observed with increasing quencher concentration for the ratio  $I_0/I$  of the fluorescence intensity with no quencher ( $I_0$ ) over that with quencher ( $I$ ) or for the ratio  $\langle\tau\rangle_0/\langle\tau\rangle$  of the number-average lifetime without quencher ( $\langle\tau\rangle_0$ ) over that with quencher ( $\langle\tau\rangle$ ). In the case where the fluorophore population can be divided into two fractions, one that is accessible to the quencher and the other that is not, the  $I_0/I$  and  $\langle\tau\rangle_0/\langle\tau\rangle$  ratios increase with increasing quencher concentration until these ratios reach a plateau at high quencher concentration. The plateau indicates that a fraction of the fluorophores continues to emit regardless of the amount of quencher being added to the solution. In essence, these fluorophores are protected from quenching. Plots of  $I_0/I$  and  $\langle\tau\rangle_0/\langle\tau\rangle$  versus quencher concentration are often referred to as Stern–Volmer plots, and in the case of protective quenching, their analysis yields  $f_a$ , the fraction of accessible fluorophores. We reasoned that the fluorescent PIMs should be good candidates to conduct fluorescence experiments, and that their high porosity should result in large  $f_a$  values if any protective quenching was taking place in these fluorescence experiments. It has been shown previously that the photoluminescence of PIM-1 solid films was quenched by nitro-aromatic vapors,<sup>11</sup> and color changes were detected by contact to various organic volatiles.<sup>12</sup>

This study describes a set of fluorescence quenching experiments that were conducted on a well-known PIM referred to as PIM-1 in the literature, which is prepared by the step-growth polymerization of 5,5',6,6'-tetrahydroxy-3,3,3',3'-tetramethylspirobisindane (TTSBI) and 2,3,5,6-tetrafluoroterephthalonitrile (TFTPN) (Scheme 1).<sup>1</sup> Analysis of the fluorescence quenching experiments required that the photo-physical behavior of the fluorescent units constituting PIM-1 be first characterized. This task was facilitated by the preparation of M-1 shown in Scheme 1 as a model compound of the fluorescent structural unit constituting PIM-1. Three often encountered fluorescence quenchers were considered in this study. The quenchers were selected depending on whether they were a proton donor (trifluoroacetic acid, TFA), an electron-rich type of quencher (tributyl amine, TBA), or an electron-poor (nitromethane,  $\text{CH}_3\text{NO}_2$ ) type of quencher. The fluorescence quenching experiments demonstrated that the interactions between PIM-1 and the quencher decreased strongly from TFA to TBA to  $\text{CH}_3\text{NO}_2$ , the latter molecule showing hardly any interactions and quenching at concen-

**Scheme 1. Chemical Structures of PIM-1 (top) and M-1 (bottom)**



trations as high as 670 mM. Whether PIM-1 was in solution or in the membrane, it was quenched in a similar manner, either by TBA or TFA, supporting the idea that the PIM-1 chains constituting the membrane are well exposed to the solvent, a result of the high porosity of the PIM-1 membrane. By demonstrating that PIMs can be probed effectively by fluorescence quenching experiments, the experiments reported herein open a new experimental means to gain additional information at the molecular level about the microstructure of PIMs.

## ■ EXPERIMENTAL SECTION

**Chemicals.** Caledon supplied HPLC grade hexanes, toluene, dichloromethane, acetone, methanol, ethanol, and distilled in glass dioxane, tetrahydrofuran, and *N,N*-dimethylformamide. Spectrograde ethyl acetate was obtained from Honeywell. Trifluoroacetic acid, nitromethane, and tributyl amine were purchased from Aldrich. The synthesis of PIM-1<sup>26</sup> and the monomer M-1<sup>27</sup> has been described earlier.

**Absorption Measurements.** A Cary 100 UV–vis spectrophotometer was used for the acquisition of all absorption spectra using a UV cell having a 1 cm path length.

**Sample Preparation for the Fluorescence Experiments.** The fluorescence spectra and decays were acquired with non-degassed solutions. The right-angle geometry was used to monitor the fluorescence of the M-1 and PIM-1 solutions in all organic solvents studied.<sup>25</sup> Fluorescence quenching experiments with TBA and TFA were conducted at room temperature (23 °C at Waterloo) and 1.5 °C. For the low temperature experiments, the sample was left to equilibrate for 30 min before a fluorescence spectrum or decay was acquired. The quenching experiments with the PIM-1 membrane were carried out at room temperature only. Hexane was selected to study the fluorescence of the PIM-1 membrane, as it is a non-solvent for PIM-1. The membrane was cut into strips which were fitted against the front window of a triangular fluorescence cell. Glass beads were loaded into the cell at the back of the membrane to hold the membrane into position. The level of the glass beads was kept lower than the position of the fluorescence spot generated by the fluorometer. A known quantity of hexane was introduced into the cell to immerse the membrane, and the quencher was added via a 100  $\mu\text{L}$  syringe to obtain various quencher concentrations in hexane. After each quencher injection, the setup was allowed to equilibrate for 5 min before a fluorescence spectrum and decay were acquired. This equilibration period was found to be sufficient by monitoring the response of the setup over time until the fluorescence signal reached a constant value. Between two

quencher additions, the fluorescence triangular cell was sealed with a Teflon cap to prevent evaporation of the solvent. The fluorescence spectra and decays acquired with the PIM-1 membrane were recorded with the front-face geometry.<sup>25</sup>

**Steady-State Fluorescence.** A PTI fluorometer equipped with an Ushio UXL-75Xe Xenon arc lamp and PTI 814 photomultiplier detection system was used to acquire the fluorescence spectra.

**Time-Resolved Fluorescence Measurements.** The fluorescence decays were acquired with 20 000 counts at the maximum of the instrument response function (IRF) and the decay on an IBH time-resolved fluorometer equipped with a nano-LED light source. A Ludox solution was used at the excitation wavelength to determine the IRF which was convoluted with a sum of exponentials whose expression is given in eq 1 for the decay analysis. The full width at half-maximum (fwhm) of the IRF equals 0.86 ns. Sums with  $n = 1-3$  exponentials were used in this study.

$$[D^*]_t = [D^*]_{t=0} \times \sum_{i=1}^n a_i \times \exp(-t/\tau_i) \quad (1)$$

The pre-exponential factors ( $a_i$ ) and decay times ( $\tau_i$ ) were obtained by least-squares optimization of the fluorescence decays using the Marquardt–Levenberg algorithm.<sup>28</sup> The quality of the fits was estimated from the  $\chi^2$  value ( $<1.30$ ), the random distribution of the residuals, and the autocorrelation of the residuals.

## RESULTS AND DISCUSSION

**Photophysical Behavior of M-1.** The fluorescence spectra of M-1 acquired in solvents having different polarities are shown in Figure 1. M-1 experienced strong Stokes shifts when

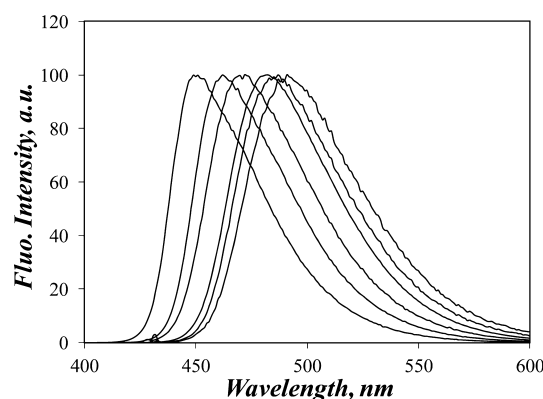


**Figure 1.** Normalized steady-state fluorescence spectra of M-1 in six organic solvents at 23 °C. From left to right in terms of increasing dielectric constant: hexane ( $\lambda_{\text{ex}} = 422$  nm), ethyl ether ( $\lambda_{\text{ex}} = 425$  nm), ethyl acetate ( $\lambda_{\text{ex}} = 426$  nm), dichloromethane ( $\lambda_{\text{ex}} = 433$  nm), dimethylformamide ( $\lambda_{\text{ex}} = 431$  nm), and dimethyl sulfoxide ( $\lambda_{\text{ex}} = 433$  nm).  $[M-1] = 4.4 \times 10^{-5}$  M.

dissolved in solvents with different polarities. The spectra were acquired in hexane (dielectric constant ( $\epsilon$ ) = 1.89), ethyl ether ( $\epsilon$  = 4.27), ethyl acetate ( $\epsilon$  = 6.08), dichloromethane ( $\epsilon$  = 8.93), dimethylformamide ( $\epsilon$  = 36.7), and dimethyl sulfoxide ( $\epsilon$  = 47.2). They were normalized at their peak maximum.<sup>29</sup> The fluorescence spectrum of M-1 was more red-shifted as the solvent polarity increased (from hexane to dimethyl sulfoxide).

The significant shift of the emission spectra shown in Figure 1 is due to a change in solvent polarity. To better characterize this effect, Lippert's equation was applied.<sup>25</sup> Lippert's equation describes changes in the energy difference between the ground and excited states of fluorophores, also known as Stokes shift. Lippert's equation is given in eq 2.

$$\nu_a - \nu_f = \frac{2}{hc} \left( \frac{\epsilon - 1}{2\epsilon + 1} - \frac{n^2 - 1}{2n^2 + 1} \right) \frac{(\mu_E - \mu_G)^2}{a^3} + \text{const} \quad (2)$$

In eq 2,  $h$  is Planck's constant,  $c$  is the speed of light, and  $a$  is the radius of the solvent cavity in which the fluorophore resides. The wavenumbers of the absorption and the emission given in  $\text{cm}^{-1}$  are  $\nu_a$  and  $\nu_f$ , respectively, and are taken as the maximum of the absorption and fluorescence spectra. The orientation polarizability ( $\Delta f$ ) is defined by the term in eq 2 involving the dielectric constant and the refractive index of the solvents. The refractive index enables the redistribution of the electrons in the fluorophore. The dielectric constant depends on both the redistribution of the electrons and the reorganization of the solvent molecules around the excited fluorophore. Thus, the effects due to electron redistribution cancel out in the expression of  $\Delta f$  so that Lippert's equation accounts essentially for the reorientation of the solvent molecules.

Figure 2 shows Lippert's plot for M-1 in 14 organic solvents. The parameters used to determine the Stokes shifts and

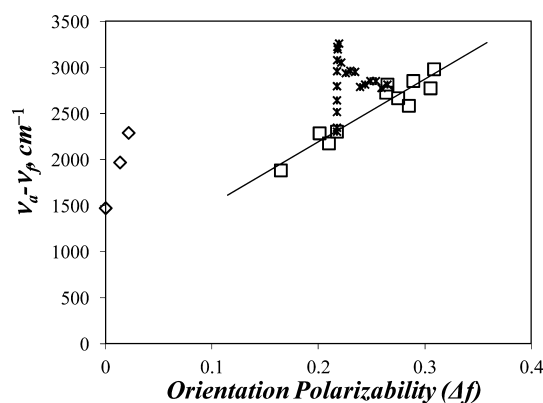


**Figure 2.** Lippert plot for M-1 in 14 solvents at 23 °C. The data points (□) are fitted linearly for  $\Delta f$  values larger than 0.15. The diamonds obtained for hexane, toluene, and dioxane could not be fitted to the Lippert plot. Crosses are for mixtures of DCM and TFA.

orientation polarizabilities are listed in Table S1 in the Supporting Information. The  $\epsilon$  and  $n$  values of the pure solvents were obtained from the literature.<sup>29</sup> Two regions can be defined in Figure 2 on the basis of the orientation polarizability of the solvent. For  $\Delta f$  values larger than 0.15,  $\nu_a - \nu_f$  increases linearly with increasing  $\Delta f$ . The slope of this straight line was found to be equal to  $6800 \pm 800 \text{ cm}^{-1}$ . Stokes shifts obtained for solvents with  $\Delta f$  values smaller than 0.03 (i.e., hexane, toluene, and dioxane which are low polarity solvents) did not follow the trend shown in Figure 2.

Since the fluorescence of M-1 is so sensitive to the solvent (Figure 1), it was important to monitor the effect that the addition of relatively large quantities of quencher (up to 670 mM in the case of  $\text{CH}_3\text{NO}_2$ ) would have on the fluorescence spectra. The fluorescence spectra obtained upon addition of different amounts of quencher to the solutions of M-1 and

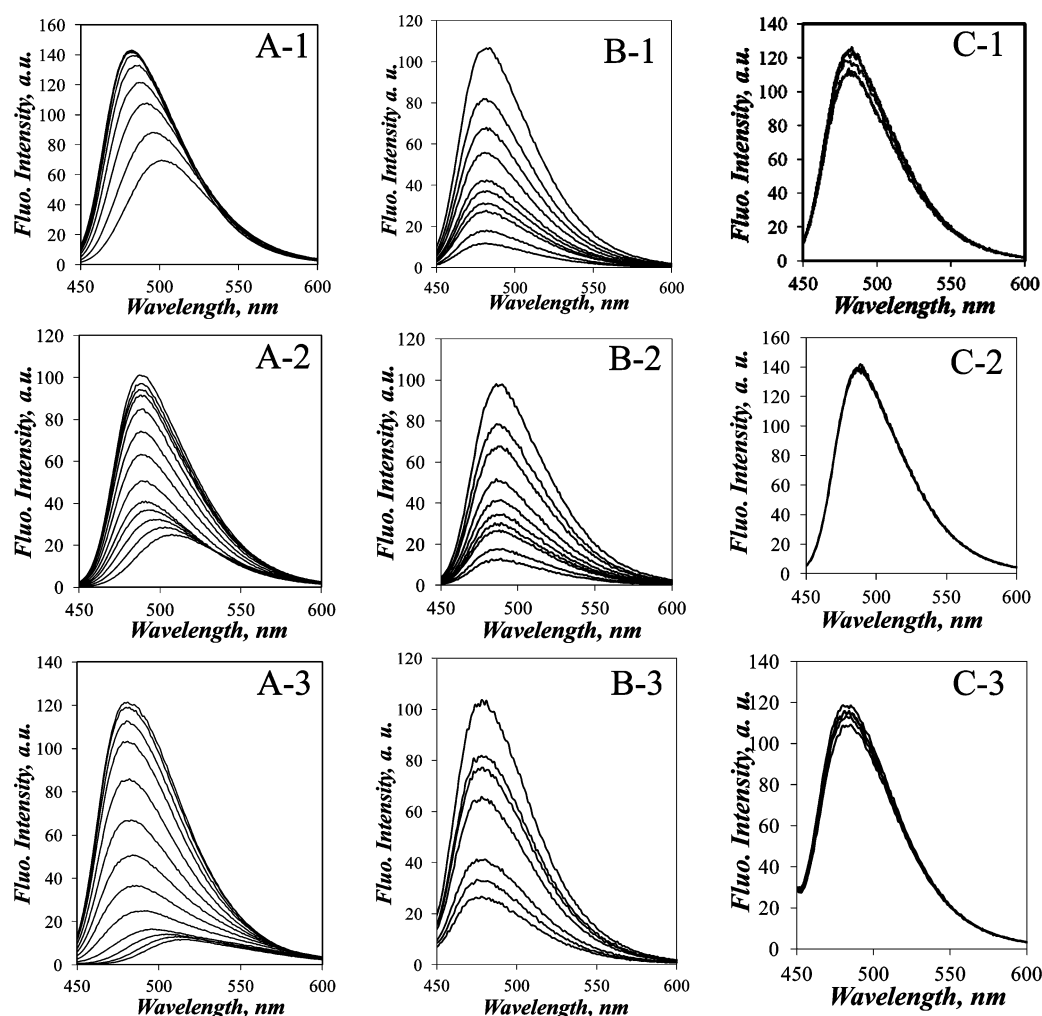


**Figure 3.** Fluorescence spectra at room temperature ( $T = 23\text{ }^{\circ}\text{C}$ ) of (1) M-1 in DCM ( $[M-1] = 4.4 \times 10^{-5}\text{ M}$ ,  $\lambda_{\text{ex}} = 433\text{ nm}$ ), (2) PIM-1 in DCM ( $[PIM-1] = 0.02\text{ g}\cdot\text{L}^{-1} = 4.4 \times 10^{-5}\text{ M}$  (in terms of structural units);  $\lambda_{\text{ex}} = 438\text{ nm}$ ), and (3) PIM-1 membrane in hexane ( $\lambda_{\text{ex}} = 422\text{ nm}$ ). (A) Quenching with TFA, (B) quenching with TBA, and (C) quenching with  $\text{CH}_3\text{NO}_2$ .

PIM-1 in DCM or for the PIM-1 membrane in hexane are shown in Figure 3. Rapid inspection of the trends shown in Figure 3 indicates that addition of TFA induces a red-shift of the fluorescence spectra. Consequently, the specific effect that addition of TFA to dichloromethane had on the fluorescence spectrum of M-1 was carefully investigated.

**Specific Solvent Effects Observed with TFA.** Although TFA ( $\epsilon = 8.42$ ) and DCM ( $\epsilon = 8.93$ ) have similar dielectric constants, their different refractive index of 1.424 for DCM and 1.285 for TFA leads to different orientation polarizabilities ( $\Delta f$ ), resulting in a substantial shift of 16 nm for the position of the absorbance maximum and 33 nm for the position of the fluorescence maximum. The fluorescence spectra of M-1 in DCM obtained upon addition of TFA to the solution are shown in Figure 3A-1, and the parameters used to determine the Stokes shifts are listed in Table S2 (Supporting Information).

For TFA concentrations ranging from 0.0 to 1.4 mM, all fluorescence spectra of M-1 overlapped perfectly, indicating that the presence of TFA did not affect the fluorescence of M-1 in this concentration range. For TFA concentration strictly greater than 1.4 mM, M-1 emits at higher wavelengths and undergoes quenching with increasing TFA concentration. Thus, an upper limit in TFA concentration of 1.4 mM seems to exist

below which the presence of TFA has no effect on the fluorescence spectrum of M-1 in terms of position of the fluorescence maximum and fluorescence intensity.

The addition of TFA to the solution of M-1 in DCM results in specific solvent effects,<sup>25</sup> as can be seen in Figure S1 in the Supporting Information. Addition of less than 1 vol % of TFA to the solution of M-1 in DCM equivalent to a TFA concentration of  $0.13\text{ mol}\cdot\text{L}^{-1}$  hardly changes the dielectric constant and refractive index of DCM. However, addition of such a minute amount of TFA shifts the fluorescence maximum of M-1 by 24 nm. The effect is much less pronounced on the absorption spectrum of M-1 in DCM that shifts by only 2 nm with 1 vol % of TFA. This discrepancy between the response of absorption and fluorescence with regard to the presence of TFA is a consequence of the time scale over which absorption ( $\sim 10^{-15}\text{ s}$ ) and fluorescence ( $\sim 10^{-8}\text{ s}$ ) take place.<sup>25</sup> Absorption occurs so quickly that neither the solvent nor the fluorophore has time to relax. Fluorescence being a slower process enables the solvent and fluorophore to relax before emission takes place, resulting in a less energetic transition occurring at a higher wavelength. The specific solvent effects that exist between M-1 and TFA in DCM were also observed in the Lippert plot shown in Figure 2 where  $\nu_a - \nu_f$  of the TFA/DCM mixtures was plotted as a function of  $\Delta f$  which was estimated

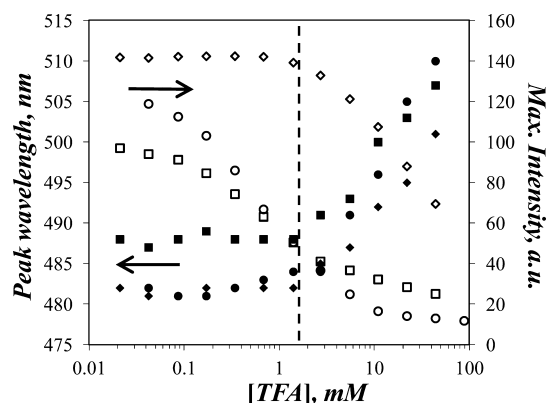


by using eqs 3 and 4 to determine the dielectric constant ( $\epsilon_{\text{mix}}$ )<sup>30,31</sup> and refractive index ( $n_{\text{mix}}$ )<sup>32</sup> of the mixtures. In eqs 3 and 4,  $f_{\text{DCM}}$  and  $f_{\text{TFA}}$  ( $=1 - f_{\text{DCM}}$ ) represent the volume fractions of DCM and TFA, respectively.

$$\epsilon_{\text{mix}} = f_{\text{DCM}} \epsilon_{\text{DCM}} + f_{\text{TFA}} \epsilon_{\text{TFA}} \quad (3)$$

$$n_{\text{mix}}^2 = f_{\text{DCM}} n_{\text{DCM}}^2 + f_{\text{TFA}} n_{\text{TFA}}^2 \quad (4)$$

Even for a volume fraction of TFA of  $2 \times 10^{-4}$  corresponding to a TFA concentration of 2.7 mM, the fluorescence spectrum of M-1 exhibits a Stokes shift ( $\Delta\nu = 2519 \text{ cm}^{-1}$ ) which is substantially larger than that in pure DCM ( $\Delta\nu = 2305 \text{ cm}^{-1}$ ). This significant increase in Stokes shift observed for small  $f_{\text{TFA}}$  values cannot be attributed to a change in the orientation polarizability of the solvent but rather to some specific interactions between TFA and M-1.<sup>25</sup> Similar specific solvent effects have already been observed with other solvent/fluorophore pairs such as between ethanol and 2-anilino-naphthalene dissolved in cyclohexane<sup>33</sup> and between THF and ellipticine dissolved in hexane.<sup>34</sup> The dependency of the intensity and wavelength at the fluorescence maximum with TFA concentration is summarized in Figure 4 for M-1 in DCM.



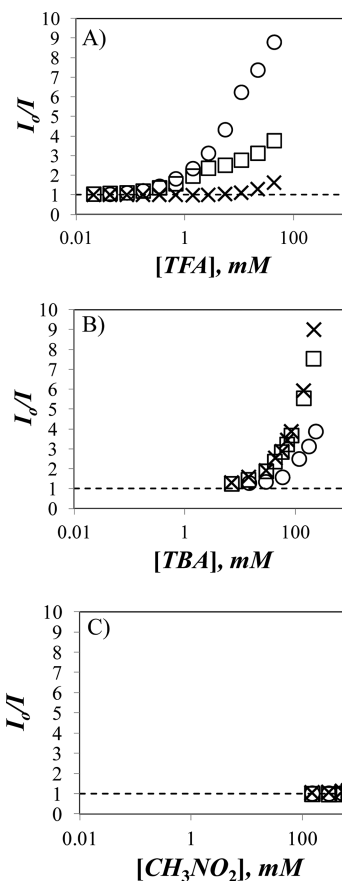
**Figure 4.** Plot of peak wavelength (filled symbols) and maximum fluorescence intensity (hollow symbols) as a function of TFA concentration for M-1 in DCM (diamond), PIM-1 in DCM (squares), and PIM-1 membrane in hexane (circles). The vertical dashed line represents a TFA concentration of 1.4 mM above which TFA affects the solvent properties of DCM.  $T = 23^\circ\text{C}$ .

Figure 4 indicates that, for TFA concentration smaller than or equal to 1.4 mM, the position of the fluorescence spectrum maximum does not change and equals 482, 488, and 482 nm for M-1 in DCM, PIM-1 in DCM, and the PIM-1 membrane in hexane, respectively. While M-1 is not being quenched in this range of TFA concentration, the fluorescence intensities of PIM-1 in DCM and membrane in hexane underwent some quenching. Although increased quenching occurs at TFA concentrations greater than or equal to 1.4 mM, the quenching is accompanied by a red-shift in the fluorescence spectra that complicates the analysis of the fluorescence data. Consequently, only fluorescence data obtained at TFA concentrations smaller than or equal to 1.4 mM were considered for more detailed analysis.

#### Fluorescence Quenching by TFA, TBA, and $\text{CH}_3\text{NO}_2$ .

The fluorescence spectra shown in Figure 3 were analyzed by plotting the ratio of the fluorescence intensity at the spectrum maximum without quencher over that with quencher, namely, the  $I_0/I$  ratio, as a function of quencher concentration in Figure

5. The electron-poor quencher  $\text{CH}_3\text{NO}_2$  was found to be the least efficient quencher for the M-1 monomer. If one considers



**Figure 5.**  $I_0/I$  ratio at  $23^\circ\text{C}$  as a function of the concentration of (A) TFA, (B) TBA, and (C)  $\text{CH}_3\text{NO}_2$  for M-1 in DCM (x), PIM-1 in DCM (□), and PIM-1 membrane in hexane (○).

a small  $I_0/I$  ratio of 1.20 to represent the onset of quenching for a given quencher, the M-1 solution in DCM required a quencher concentration of 900, 6, and 13 mM for, respectively,  $\text{CH}_3\text{NO}_2$ , TBA, and TFA to reach an  $I_0/I$  ratio of 1.20. The poor quenching efficiency found for the electron-poor  $\text{CH}_3\text{NO}_2$  might have been expected after noting that the cyano substituents of M-1 in Scheme 1 pull the electrons away from M-1, making it less sensitive to quenching by  $\text{CH}_3\text{NO}_2$ .

This result, together with the fact that  $\text{CH}_3\text{NO}_2$  did not quench PIM-1 in DCM and the PIM-1 membrane in hexane, led us to discard  $\text{CH}_3\text{NO}_2$  as a quencher for the remainder of this study. Quenching of M-1 by the electron-rich TBA was much stronger, occurring at TBA concentrations 2 orders of magnitude larger than those for  $\text{CH}_3\text{NO}_2$ .

The  $I_0/I$  ratios obtained in Figure 5 clearly supported that, as alluded to earlier, specific solvent effects were occurring between PIM-1 and TFA. If an  $I_0/I$  ratio of 1.20 was taken to represent the onset of quenching, an onset TFA concentration of 0.17 mM was required to quench PIM-1 in DCM, a quencher concentration almost 2 orders of magnitude smaller than the onset concentration of 6.3 mM obtained with TBA. The enhanced ability of PIM-1 in DCM to be quenched by TFA was also observed for the PIM-1 membrane in hexane. Only 0.17 mM TFA was needed to reach an  $I_0/I$  ratio of 1.20 for the PIM-1 membrane in hexane compared to 16 mM TBA.

Similar conclusions were reached for solutions of PIM-1 in DCM quenched by TFA and TBA at 1.5 °C. The results obtained for the fluorescence quenching of PIM-1 with TBA and TFA are discussed in more detail hereafter.

Although it might seem surprising that TFA binds to the polymer (PIM-1) but not to the monomer (M-1), such effects are often encountered in polymer science where binding effects are enhanced by polymeric systems. For instance, the hydrophobic dye pyrene is known to interact with the surfactant sodium dodecyl sulfate (SDS) after SDS forms micelles above its critical micellar concentration (CMC). However, water-soluble polymers labeled with pyrene interact with SDS at SDS concentrations that are lower than the CMC of SDS, because these polymers form pyrene aggregates of greater hydrophobicity than a pyrene monomer, and these pyrene aggregates are selectively targeted by the SDS molecules.<sup>35</sup> A similar effect is certainly at play to explain the different interactions that take place between TFA and the M-1 monomer and the PIM-1 polymer.

**Quenching of PIM-1 by TBA.** The fluorescence decays of each solution used for the fluorescence spectra in Figure 3B were acquired. They were fitted with a sum of exponentials according to eq 1 to determine the number-average decay time  $\langle\tau\rangle$ . The decay times and pre-exponential factors retrieved from this analysis are listed in Tables S3–S7 (Supporting Information). M-1 decayed monoexponentially in DCM, the fluorescence decay becoming biexponential at higher TBA concentrations. PIM-1 in DCM exhibited a slightly biexponential decay with a long decay time of 10.8 ns retrieved with 91% of the pre-exponential weight. This decay time is close to the 11.8 ns lifetime of M-1 in DCM. The fact that the long decay time in the PIM-1 decay was retrieved with a pre-exponential weight close to unity suggests that the M-1 units constituting the PIM-1 backbone are locally excited and undergo little interaction with each other in solution despite the residual overlap between the absorption and fluorescence spectra that could potentially lead to energy migration (see Figure S2, Supporting Information).

The ratios  $I_0/I$  and  $\langle\tau\rangle_0/\langle\tau\rangle$ , where the subscript “o” refers to the solution without quencher, were calculated and plotted as a function of TBA in Figure 6. The  $I_0/I$  and  $\langle\tau\rangle_0/\langle\tau\rangle$  ratios obtained with M-1 and PIM-1 in DCM clustered around a single straight line, while a line with a smaller slope was obtained for the  $I_0/I$  and  $\langle\tau\rangle_0/\langle\tau\rangle$  ratios determined for the PIM-1 membrane in hexane.

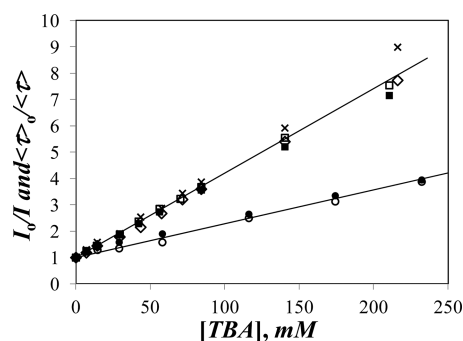


**Figure 6.**  $I_0/I$  (filled symbols and crosses) and  $\langle\tau\rangle_0/\langle\tau\rangle$  (open symbols) ratios plotted as a function of TBA concentration for M-1 in DCM (crosses and diamonds), PIM-1 in DCM (squares), and PIM-1 membrane in hexane (circles).  $T = 23$  °C.

For each sample, similar trends were obtained between steady-state (SSF) and time-resolved (TRF) fluorescence, demonstrating lack of static quenching. The straight lines obtained by SSF and TRF for the Stern–Volmer plots indicate that quenching by TBA is collisional in nature whereby an excited fluorescent M-1 unit must collide in a dynamic manner with a TBA molecule to result in quenching. At first glance, the steeper slopes obtained in Figure 6 for the quenching of M-1 and PIM-1 in DCM would suggest that quenching of these samples by TBA is more efficient than for the PIM-1 membrane. However, the lifetime of the fluorescent species needs to be taken into account, as the slope of a Stern–Volmer plot equals the product  $k_Q \times \langle\tau\rangle_0$  and, thus, is affected by the value of  $\langle\tau\rangle_0$ .

The fluorescence decay of the PIM-1 membrane in hexane had a long decay time of 5.5 ns obtained with a pre-exponential contribution of 84%. Whereas PIM-1 in DCM had a lifetime of 10.6 ns similar to that of 11.8 ns for M-1 in DCM, the long decay time of 5.5 ns obtained for the PIM-1 membrane in hexane is much shorter than the lifetime of 9.0 ns found for M-1 in hexane. It can be hypothesized that, in the bulk, the M-1 units constituting the PIM-1 backbone are affected by other polymer chains. The shorter lifetime could indicate that packing forces in the membrane lead to bending of M-1 at the ether bonds, resulting in a loss of planarity and a shorter decay time. These observations are supported by conclusions drawn from atomic packing models used to mimic the PIM-1 membrane which demonstrated a certain out-of-plane flexibility of the ladder part of the PIM-1 chain around the dioxane ring.<sup>36</sup> In any case, the determination of  $\langle\tau\rangle_0$  for the PIM-1 membrane allowed the determination of the quenching rate constant  $k_Q$  from the different slopes shown in Figure 6. The  $k_Q$  values are reported in Table 1.

**Table 1.** Average Lifetime  $\langle\tau\rangle_0$  and Bimolecular Quenching Rate Constants Obtained by SSF and TRF for the Quenching of Solutions of M-1 and PIM-1 in DCM and PIM-1 Membrane in Hexane

	$T$ (°C)	$\langle\tau\rangle_0$ (ns)	$k_Q$ obtained by SSF ( $\times 10^{-9} \text{ M}^{-1}\text{s}^{-1}$ )	$k_Q$ obtained by TRF ( $\times 10^{-9} \text{ M}^{-1}\text{s}^{-1}$ )
M-1 in DCM	23	11.8	3.11 ( $\pm 0.06$ )	2.68 ( $\pm 0.03$ )
	1.5 <sup>a</sup>	11.8	2.28 ( $\pm 0.07$ )	1.89 ( $\pm 0.06$ )
PIM-1 in DCM	23	10.3	3.06 ( $\pm 0.03$ )	2.87 ( $\pm 0.02$ )
	1.5 <sup>a</sup>	10.0	2.91 ( $\pm 0.03$ )	2.56 ( $\pm 0.04$ )
PIM-1 membrane in hexane	23	5.1	2.41 ( $\pm 0.08$ )	2.41 ( $\pm 0.09$ )

<sup>a</sup>A degassing cell was used for the TBA quenching experiments at 1.5 °C.

The rate constants  $k_Q$  obtained by SSF and TRF are comparable and large, supporting the notion that little static quenching is present and that TBA is an efficient quencher, respectively. The  $k_Q$  and  $\langle\tau\rangle_0$  values are similar for M-1 and PIM-1 in DCM for a given temperature, suggesting that the fluorophore is locally excited, that the excitation does not travel along the polymer, and that the fluorescent units in PIM-1 are fully accessible to the solvent, certainly a result of the inherently open structure of PIM-1. The  $k_Q$  values of  $2.4 \times 10^9 \text{ s}^{-1}$  obtained for the PIM-1 membrane in hexane, a nonsolvent for PIM-1, are decreased by only  $\sim 20\%$  when compared to the  $k_Q$  value for PIM-1 in DCM, indicating that the fluorescent units

in the PIM-1 membrane are also fully accessible and effectively quenched, again a consequence of the presence of micropores in the polymer matrix.

When the quenching experiments with TBA were repeated at 1.5 °C, hardly any quenching was first observed. Since protonation of a tertiary amine reduces its quenching ability substantially,<sup>37</sup> we suspected that protonation of TBA could be happening in DCM at 1.5 °C, a temperature low enough to favor the condensation of air moisture laden with carbonic acid. The fluorescence cell was then replaced by a degassing cell where the quartz fluorescence cell is connected to the outside by an airtight stopcock via a quartz-to-pyrex graded seal. The outside opening was sealed with a rubber septum, and TBA was injected through the septum into the DCM solution placed in the degassing cell via a gastight syringe. Using the degassing cell, TBA quenching was observed at 1.5 °C (see Figures S3 and S4, Supporting Information). Depending on the entry in Table 1, the rate constant  $k_Q$  decreased by 5–40% when the temperature was lowered from 23 to 1.5 °C. The decrease was more pronounced for the monomer M-1 (~40%) than for the polymer PIM-1 (~10%). Differences in  $k_Q$  value as a function of temperature can be due to a number of reasons which include how temperature affects the probability of quenching upon contact between a fluorophore and its quencher. However, the decrease in  $k_Q$  observed with decreasing temperature can also be rationalized, in part, by considering that the viscosity of DCM increased by 20% from 0.42 to 0.52 mPa·s upon lowering the temperature from 23 to 1.5 °C. The increase in viscosity is expected to affect quenching if it occurs by diffusion, as the data provided in Figure 6 and Figure S3 (Supporting Information) suggest that it does for TBA. Unfortunately, the use of the degassing cell with its long neck for the quenching experiments conducted with TBA at 1.5 °C prevented us from repeating these measurements with the PIM-1 membrane in hexane, as it was impossible to introduce the strip of membrane through the long neck of the cell.

**Quenching of PIM-1 by TFA.** The fluorescence quenching experiments conducted with TBA were repeated with TFA at 1.5 and 23 °C. The results obtained at room temperature are discussed first. The fluorescence decays of the different samples were acquired and fitted with sums of exponentials to obtain the  $\langle\tau\rangle_0/\langle\tau\rangle$  ratios. They were plotted as a function of TFA concentration in Figure 7, together with the  $I_0/I$  ratios. The pre-exponential factors and decay times retrieved from this analysis are listed in Tables S8–S12 (Supporting Information).

For TFA concentrations smaller than 22 mM, the fluorescence decays of M-1 in DCM were monoexponential. The lifetime of M-1 in DCM remained constant and equaled 11.5 ns up to a TFA concentration of 2.7 mM. For TFA concentrations larger than 2.7 mM, the lifetime of M-1 decreased with increasing TFA concentration. The fluorescence decay of M-1 became slightly biexponential for the highest TFA concentration studied of 43.8 mM. When the ratio  $\tau_0/\tau$  of the lifetime of the solution without ( $\tau_0$ ) and with ( $\tau$ ) quencher was plotted as a function of TFA concentration in Figure 7, it overlapped perfectly the trend obtained with the  $I_0/I$  ratio. This overlap demonstrates the absence of association between TFA and M-1 in the ground state, as no static quenching is observed.

Solutions of PIM-1 in DCM behaved differently from those of M-1 upon addition of TFA. Whereas addition of up to 1.4 mM TFA to the M-1 solution in DCM had no effect on the fluorescence spectrum of M-1, the fluorescence intensity of PIM-1 in Figure 3A-2 decreased substantially with increasing

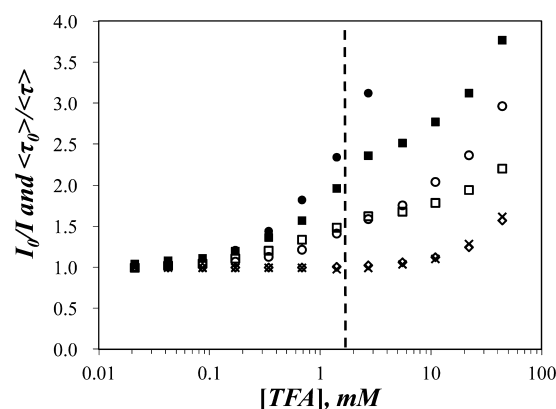


**Figure 7.** Plot of  $I_0/I$  (filled symbols and crosses) and  $\langle\tau\rangle_0/\langle\tau\rangle$  (empty symbols) at  $T = 23$  °C as a function of TFA concentration for M-1 in DCM (diamonds and crosses), PIM-1 in DCM (squares), and PIM-1 membrane in hexane (circles). The vertical dashed line represents a TFA concentration of 1.4 mM above which TFA affects the solvent properties of DCM or hexane for the PIM-1 solution and PIM-1 membrane, respectively.

TFA concentration but the fluorescence spectrum of PIM-1 did not shift. Since the concentration of M-1 in DCM is equal to that of the structural units constituting PIM-1 and since the presence of TFA did not affect the fluorescence of M-1 for TFA concentrations as large as 1.4 mM, these results suggest that TFA binds to PIM-1. Since the amount of TFA in the solution is small, the presence of TFA at such low concentration does not affect the solvent properties and the fluorescence spectrum of PIM-1 is not red-shifted. The decrease in fluorescence intensity reflects quenching of PIM-1 by bound TFA. For TFA concentrations larger than 2.7 mM, the behavior of PIM-1 in DCM is similar to that of M-1. Larger TFA concentrations affect the solvent properties, and the fluorescence spectrum of PIM-1 in DCM is red-shifted and the fluorescence intensity decreases further. These results were summarized in Figure 4.

The fluorescence decays of PIM-1 in DCM were acquired and fitted with a sum of two exponentials. The pre-exponential factors and decay times retrieved from the fits are listed in Table S10 in the Supporting Information. The number average lifetime of PIM-1 in DCM with ( $\langle\tau\rangle$ ) and without ( $\langle\tau\rangle_0$ ) TFA was calculated for different TFA concentrations, and the ratio  $\langle\tau\rangle_0/\langle\tau\rangle$  was plotted as a function of TFA concentration in Figure 7 along with the ratio  $I_0/I$  obtained from the steady-state fluorescence spectra shown in Figure 3A-2. Both  $\langle\tau\rangle_0/\langle\tau\rangle$  and  $I_0/I$  increased with increasing TFA concentration, reflecting dynamic fluorescence quenching. However, whereas they overlapped perfectly for M-1 in Figure 7, the  $I_0/I$  ratio was larger than the  $\langle\tau\rangle_0/\langle\tau\rangle$  ratio for PIM-1 in DCM. This observation indicates that static quenching is taking place<sup>25</sup> where TFA binds to PIM-1 and quenches its structural units quasi-instantaneously on a time-scale that is too fast to be detected in our time-resolved fluorescence decays. The existence of static quenching for PIM-1 in the presence of TFA is clear evidence that TFA binds to PIM-1 dissolved in DCM.

The spectral shifts seen with PIM-1 in DCM when increasing amounts of TFA are added to the solution could be due to excimer formation whereby the blue-shifted monomer would be quenched more efficiently by TFA than the red-shifted excimer, thus inducing the red-shift observed in the fluorescence spectra upon addition of TFA. Although excimer



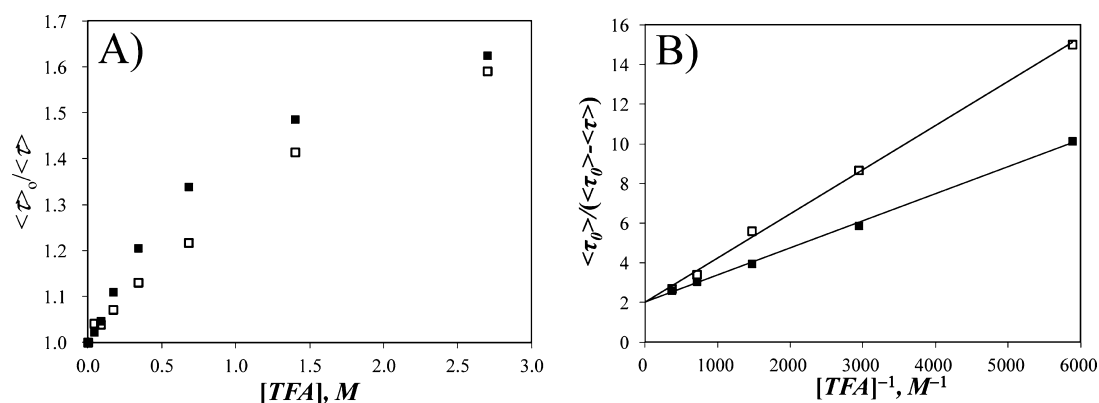


**Figure 8.** (A) Plot of  $\langle\tau\rangle_0/\langle\tau\rangle$  versus TFA concentration. (B) Plot of  $\langle\tau\rangle_0/(\langle\tau\rangle_0 - \langle\tau\rangle)$  versus TFA concentration. PIM-1 in DCM (■) and PIM-1 membrane in hexane (□);  $T = 23\text{ }^{\circ}\text{C}$ .

formation is unlikely for M-1 since it decays monoexponentially at a concentration of  $4.4 \times 10^{-5}\text{ M}$ , the local concentration of aromatic structural units in the polymer coil of PIM-1 in DCM is much larger than the equivalent concentration of structural units also equal to  $4.4 \times 10^{-5}\text{ M}$ . Such high local concentrations could lead to excimer formation between an excited and a ground-state structural unit. Since the excimer fluorescence decay would exhibit different features from the monomer with a rise time at the early times of the decay, fluorescence decays of PIM-1 in DCM were acquired at emission wavelengths of 470, 480, 490, 500, and 510 nm to look for different regions of the fluorescence spectrum where the excimer might emit. All fluorescence decays overlapped (see Figure S5, Supporting Information), and no rise time could be detected. This result indicates that the decays of PIM-1 in DCM retain the same features as a function of wavelength which suggests absence of excimer formation.

**Quenching of PIM-1 Membrane in Hexane by Trifluoroacetic Acid.** The microporosity of PIM-1 membranes has been characterized by a number of techniques. Positron annihilation lifetime spectroscopy has been used to determine the pore radius of a PIM-1 membrane which was found to be equal to 0.48 nm, yielding an average volume of  $0.47\text{ nm}^3$ .<sup>24</sup> The surface area of PIM-1 matrixes depends on aging and varies between 600 and more than 1000  $\text{m}^2/\text{g}$  as determined by the BET method using  $\text{N}_2$  at 77 K.<sup>36</sup> To study the interactions between the PIM-1 membrane and TFA, hexane was selected, as it is a nonsolvent for PIM-1. The PIM-1 membrane was placed against the wall of the fluorescence cell and maintained in place by adding glass beads at the back of the membrane. The fluorescence cell was filled with hexane to immerse the PIM-1 membrane, and TFA aliquots were added. Upon addition of TFA, the fluorescence response of the PIM-1 membrane in hexane paralleled very closely that of PIM-1 dissolved in DCM, as can be seen in Figure 3A–3. The fluorescence spectrum did not shift for TFA concentrations smaller than 1.4 mM, but the fluorescence intensity decreased with increasing TFA concentration. As for solutions of M-1 and PIM-1 in DCM, the fluorescence spectrum of the PIM-1 membrane in hexane was red-shifted and the fluorescence intensity decreased with increasing TFA concentration for TFA concentrations greater than 2.7 mM. These trends were presented in Figure 4. A plot of  $I_0/I$  as a function of TFA concentration is shown in Figure 7.  $I_0/I$  for the PIM-1 membrane in hexane increased very strongly with increasing TFA concentration, reaching a value of 8.8 for a TFA

concentration of 43.8 mM, much larger than the  $I_0/I$  ratio of 3.8 reached by PIM-1 dissolved in DCM for the same TFA concentration. This result suggests that the PIM-1 membrane in hexane induces much greater binding of TFA to PIM-1 compared to PIM-1 in DCM. This is probably a consequence of the much larger quantity of PIM-1 present in the fluorescence cell which drives the equilibrium toward binding when dealing with the PIM-1 membrane.

Analysis of the fluorescence decays acquired with the PIM-1 membrane in hexane was carried out with a sum of exponentials. All decays were biexponential, and Table S12 in the Supporting Information presents all pre-exponential factors and decay times retrieved from the analysis. The  $\langle\tau\rangle_0/\langle\tau\rangle$  ratios were plotted in Figure 7 as a function of TFA concentration. As for PIM-1 in DCM, the  $\langle\tau\rangle_0/\langle\tau\rangle$  ratios for the PIM-1 membrane in hexane took smaller values than the  $I_0/I$  ratios, confirming the existence of static quenching between TFA and PIM-1 resulting from the binding of TFA to PIM-1.

Inspection of Tables S10 and S12 (Supporting Information) indicates that, although quenching of PIM-1 by TFA results in an enhancement of the contribution of the short decay component at the expense of the long decay component, the value of the long decay time itself is little affected by addition of TFA (from 10.6 to 9.6 ns or a 9% decrease for PIM-1 in DCM with TFA concentrations ranging from 0 to 1.4 mM and from 5.6 to 5.2 ns or a 7% decrease for the PIM-1 membrane in hexane with the same range of TFA concentrations). This suggests that protective quenching is taking place, as a dynamic quenching mechanism would shorten the long decay time more effectively as was observed for the TBA quenching experiments where the long decay time reported in Tables S3–S7 (Supporting Information) decreases strongly with increasing TBA concentration. This suggestion is supported by a plot of  $\langle\tau\rangle_0/\langle\tau\rangle$  versus TFA concentration in Figure 8A that shows that  $\langle\tau\rangle_0/\langle\tau\rangle$  does not increase linearly with increasing TFA concentration but shows a downward curvature at high TFA concentration, an indication that protective quenching is taking place.<sup>25,38,39</sup> As for the TBA experiments, the TFA quenching experiments were repeated at 1.5  $^{\circ}\text{C}$  for M-1 and PIM-1 in DCM. The results are shown in Figures S6–S8 in the Supporting Information. The trends obtained at 1.5  $^{\circ}\text{C}$  for the  $\langle\tau\rangle_0/\langle\tau\rangle$  and  $I_0/I$  ratios are similar to those obtained at 23  $^{\circ}\text{C}$ .

**Determination of the Fraction of Accessible Fluorophores,  $f_a$ .** Quenching of PIM-1 by TFA appears to be complex and proceeds via at least three mechanisms. First, TFA



binds to PIM-1, which induces static quenching as demonstrated by the different  $\langle\tau\rangle_o/\langle\tau\rangle$  and  $I_o/I$  ratios obtained as a function of TFA concentration in Figure 7. Second, PIM-1 undergoes dynamic quenching by TFA, as  $\langle\tau\rangle_o/\langle\tau\rangle$  is greater than unity at all TFA concentrations in Figure 7. Third, PIM-1 undergoes some protective quenching as  $\langle\tau\rangle_o/\langle\tau\rangle$  curves downward in Figure 6A with increasing TFA concentration. These complex photophysical processes were handled in the following manner according to a procedure that was developed earlier.<sup>39</sup>

Scheme 2 provides the framework used to derive the equations that describe mathematically the trends shown in

**Scheme 2. Photophysical Processes Undergone by a Chromophore D Subject to Static, Protective, and Dynamic Quenching<sup>39</sup>**

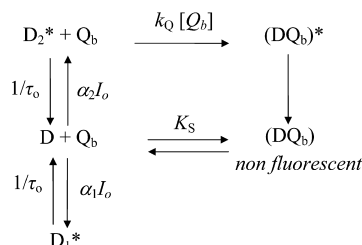
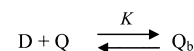


Figure 8A and B. In Scheme 2, the chromophore (D) is equivalent to the M-1 structural units constituting the PIM-1 backbone and TFA is the quencher ( $Q_b$ ) whose subscript “b” indicates that the quencher is bound to the polymer. The molar fractions  $\alpha_1$  and  $\alpha_2$  represent those repeating segments along PIM-1 which are protected and quenched diffusionaly, respectively. The fraction  $1 - \alpha_1 - \alpha_2$  represents those M-1 units in the PIM-1 backbone that are complexed with TFA and are quenched quasi-instantaneously, resulting in static quenching. The fraction of chromophores which are accessible to the quencher  $f_a$  is expressed by  $\alpha_2/(\alpha_1 + \alpha_2)$ . In this study,  $f_a$  represents the fraction of M-1 monomers that are accessible to the solvent being either DCM for the PIM-1 solution or hexane for the PIM-1 membrane. Those repeating units that are not exposed to the solvent are in effect “protected” from the TFA quencher. Dynamic quenching of the polymer occurs with a rate constant  $k_Q$  and  $K_S$  is the equilibrium constant for the formation of the complex between PIM-1 and TFA. The unquenched lifetime of PIM-1 is described by  $\tau_o$  in Scheme 2.

Dynamic quenching usually occurs when the encounter between a quencher in solution and an excited chromophore is controlled by diffusion. However, TFA does not quench M-1 in DCM at concentrations smaller than 2 mM. This result implies that, when TFA quenches PIM-1, those TFA molecules cannot be located in the solution. Rather, TFA is already bound to PIM-1, as demonstrated by the different  $\langle\tau\rangle_o/\langle\tau\rangle$  and  $I_o/I$  ratios in Figure 7. The fact that dynamic quenching occurs implies that this quenching results from either exciton migration allowed by the residual overlap that exists between the absorption and fluorescence spectra of PIM-1 (see Figure S2, Supporting Information), diffusion of TFA inside the polymer coil in DCM or the PIM-1 matrix for the PIM-1 membrane in hexane, internal motions of the PIM-1 backbone, or a combination of all processes. Out of the four processes, exciton migration seems the least likely, however, as it would enable access of TFA to all structural units of PIM-1 and no protective quenching would be observed. Exciton migration was also ruled

out in the TBA quenching experiments which showed that the quenching of PIM-1 in DCM by TBA occurred in the same manner as that of M-1 in DCM. Regardless of the details of the quenching mechanism, the concentration of quencher bound to the polymer must be considered. This is done in Scheme 3 by assuming the existence of an equilibrium between TFA molecules free in solution and bound to PIM-1.

**Scheme 3. Equilibrium Describing the Binding of TFA to PIM-1**



Schemes 2 and 3 were used to derive eqs 5 and 6 that describe the trends shown in Figure 8A and B. Unfortunately,  $k_Q$  and  $K_S$  used to derive eqs 5 and 6 cannot be determined quantitatively because the equilibrium constant  $K$  in Scheme 3 is unknown. However, analysis of the trends shown in Figure 6B with eq 5 yields a quantitative measure of  $f_a$ .

$$\frac{\langle\tau_o\rangle}{\langle\tau_o\rangle - \langle\tau\rangle} = \frac{1}{f_a} + \frac{1}{f_a k_Q \tau_D} \times \frac{1 + K[D]}{K[D]} \times \frac{1}{[Q]} \quad (5)$$

$$\begin{aligned} \frac{I_o}{I} \left( 1 - f_a + \frac{f_a}{1 + k_Q \tau_D \frac{K[D]}{(1 + K[D])} [Q]} \right) \\ = 1 + \frac{K_S K [D]}{1 + K [D]} [Q] \end{aligned} \quad (6)$$

Since the fluorescence decays of PIM-1 were multiexponential,  $\langle\tau\rangle_o$  and  $\langle\tau\rangle$  were used in eqs 5 and 6 in lieu of  $\tau_o$  and  $\tau$ , as has been done in a number of other studies.<sup>38,39</sup>  $[D]$  is the concentration of M-1 monomers found in a DCM solution of PIM-1 or the local concentration of M-1 monomers in the PIM-1 membrane. A plot of the  $\langle\tau_o\rangle/(\langle\tau_o\rangle - \langle\tau\rangle)$  ratio as a function of  $1/[Q]$  is shown in Figure 8B for PIM-1 dissolved in DCM and the PIM-1 membrane in hexane. Two straight lines were obtained as predicted by eq 5. The intercept of the straight lines yielded  $f_a$ . In this analysis, data obtained with TFA concentrations smaller than 2 mM were considered to avoid the solvent effects that give rise to the fluorescence shift observed for M-1 in DCM, PIM-1 in DCM, and the PIM-1 membrane in hexane (Figure 3A). Unfortunately, fitting the straight lines in Figure 8B cannot retrieve  $k_Q$  and  $K_S$  used in eqs 5 and 6 because the equilibrium constant  $K$  in Scheme 3 is unknown. Furthermore,  $[D]$  cannot be easily determined for the experiments dealing with the PIM-1 membrane in hexane. Fortunately, the determination of  $f_a$  in eq 5 is not affected by these complications and it was found to be equal to  $0.50 \pm 0.04$  and  $0.50 \pm 0.08$  at 25 °C for PIM-1 dissolved in DCM and the PIM-1 membrane in hexane, respectively. When these experiments were repeated for PIM-1 in DCM quenched by TFA at 1.5 °C, an  $f_a$  value of  $0.54 \pm 0.04$  was obtained (Figure S8, Supporting Information). These values imply that ~50% of the PIM-1 repeating units are not accessible to TFA at 1.5 and 25 °C, and thus not exposed to the solvent.

**Comparison between the Fluorescence Quenching Experiments Conducted with TBA and TFA.** Dynamic collisional quenching takes place with TBA, and straight lines were obtained for the Stern–Volmer plots shown in Figure 6. These linear Stern–Volmer plots indicate that all fluorophores are fully accessible to TBA, or that  $f_a$  equals unity for the TBA

quenching of PIM-1 in DCM or the PIM-1 membrane in hexane. Quenching by TBA was also found to be very efficient occurring with large bimolecular rate constants of  $(2 - 3) \times 10^9 \text{ s}^{-1}$ . Despite TBA being an efficient quencher, TFA appears to be much more efficient still, inducing substantial quenching at TFA concentrations 2 orders of magnitude smaller than those obtained for TBA (see Figure 5). This enhanced quenching efficiency cannot be the result of random diffusive encounters between fluorophore and TFA molecules homogeneously distributed in the solution, as it would result in an impossibly large  $k_Q$  value 2 orders of magnitude larger than the already large values of  $(2 - 3) \times 10^9 \text{ s}^{-1}$  obtained for TBA. Rather, the enhanced quenching efficiency of TFA is enabled by the binding of TFA onto PIM-1 which was demonstrated by the observation of specific solvent effects in Figures 2, 3A-1, 3A-2, 3A-3, and 4 and static quenching in Figure 7. Interestingly, specific binding of TFA onto PIM-1 is enhanced by the polymer, as TFA does not appear to bind to and quench the M-1 monomer constituting the polymer up to TFA concentrations of 10 mM (see Figure 7).

The quenching of PIM-1 by TFA is unconventional, since it results in protective quenching. In the range of TFA concentrations between 0.04 and 1.4 mM, only half of the fluorescent units constituting the polymer are accessible to TFA. At higher TFA concentration, the red-shift of the PIM-1 fluorescence spectra shown in Figures 3A-2 and 3A-3 suggests that the entire polymer becomes accessible to the solvent and that it is affected by the change of polarity induced by the addition of increasing quantities of TFA. The  $f_a$  value of 0.50 retrieved for the polymer in solution indicates that about half the fluorescent units constituting the PIM-1 backbone are accessible to TFA at low TFA concentrations. That  $f_a$  is not equal to unity for these low TFA concentrations might be attributed to the inherent rigidity of the PIM-1 backbone whose dynamics are expected to be much slower than those of the solvent. These slow dynamics prevent easy access of TFA to the M-1 repeating units in solution and result in the small  $f_a$  value. On the other hand, since the PIM-1 membrane is insoluble in hexane, the solvent should have limited access to the PIM-1 matrix and a  $f_a$  value close to zero would be expected. A value of 0.5 was retrieved for  $f_a$  which indicates that a surprisingly large fraction of the units constituting the PIM-1 backbone are accessible to the solvent. These results showing high accessibility of the PIM-1 matrix to TFA and TBA agree with the known high porosity of PIM-1,<sup>1</sup> as a nonporous polymeric material would be expected to yield an  $f_a$  value equal to zero. Furthermore, the fact that  $f_a$  takes the same value for PIM-1 dissolved in DCM and the insoluble PIM-1 membrane in hexane suggests that the PIM-1 backbone adopts the same conformation in solution and in the bulk. This result is a consequence of the inherent backbone rigidity of PIM-1 which prevents the rapid molecular rearrangement of the backbone conformation in solution, at least over the less than 80 ns time scale of these fluorescence experiments (see Figure S5, Supporting Information). The relatively facile accessibility to TBA or TFA of the PIM-1 matrix in the membrane results from the high porosity of the PIM-1 membrane, which is a consequence of the high rigidity of the PIM-1 backbone. Both properties are reflected in these fluorescence quenching experiments.

## CONCLUSIONS

The photophysical properties of M-1 were carefully characterized in 14 solvents. The fluorescence spectrum of M-1 showed a clear response to the nature of the solvent (Figure 1). The photophysical parameters retrieved from the analysis of the absorption and fluorescence spectra of the M-1 solutions were well described by Lippert's equation as long as the solvents had an orientation polarizability larger than 0.15. These solvent effects needed to be taken into account when conducting quenching experiments, as addition of increasing amounts of quencher to the solution could affect the solvent, and thus the photophysical properties of M-1. The three selected quenchers were the proton-donor TFA, the electron-rich TBA, and the electron-poor  $\text{CH}_3\text{NO}_2$ . Out of these three quenchers, TFA was found to induce pronounced solvent effects. Consequently, the effect that addition of TFA aliquots to a PIM-1 solution in DCM might have to the fluorescence spectrum of PIM-1 was carefully investigated. Although specific solvent effects took place between TFA and M-1 in DCM, the fluorescence spectra of M-1 in DCM were unaffected by the presence of TFA in the solution up to a TFA concentration of 1.4 mM (Figure 4). Larger TFA concentrations induced a red-shift of the fluorescence spectra and were associated with a decrease of the fluorescence intensity. From these experiments, it was concluded that the fluorescence data obtained with the TFA quenching experiments would be interpreted only for TFA concentrations smaller than 1.4 mM.

The quenching study showed that  $\text{CH}_3\text{NO}_2$  was a poor quencher, and it was not considered any further. On the other hand, TBA was found to be an efficient quencher. The Stern–Volmer plots in Figure 6 obtained for  $I_0/I$  and  $\langle\tau\rangle_0/\langle\tau\rangle$  were linear and overlapped, indicating collisional quenching and absence of static quenching, respectively. Similar  $\langle\tau\rangle_0$  and  $k_Q$  values were retrieved for solutions of M-1 and PIM-1 in DCM that suggested a locally excited chromophore. Similar results were obtained at 1.5 and 23 °C, suggesting that temperature had little effect on these experiments. A shorter  $\langle\tau\rangle_0$  value was obtained for the PIM-1 membrane that indicated that the planar conformation of the M-1 structural units is affected by the presence of the PIM-1 chains in the PIM-1 matrix, probably resulting in a bending of the M-1 unit at the ether bonds. Nevertheless, a large  $k_Q$  value was recovered for the quenching of the PIM-1 membrane by TBA, similar in magnitude to those obtained for the quenching of the M-1 and PIM-1 solutions in DCM. This result suggests high accessibility of the polymer structural units to TBA.

Quenching of PIM-1 by TFA in DCM was probed. Up to a TFA concentration of 1.4 mM, the fluorescence spectra of PIM-1 in DCM did not shift but showed a pronounced decrease in fluorescence intensity with increasing TFA concentration. Larger TFA concentrations induced a red-shift of the fluorescence spectra. Contrary to M-1 in DCM, PIM-1 in DCM underwent static quenching, as demonstrated by the comparison of the  $I_0/I$  and  $\langle\tau\rangle_0/\langle\tau\rangle$  ratios in Figure 7. Analysis of the fluorescence decays indicated the existence of protective quenching. Similar observations were made for a PIM-1 membrane immersed in hexane.

Analysis of the fluorescence data obtained for PIM-1 in DCM and the PIM-1 membrane in hexane yielded the fraction of M-1 monomers in the PIM-1 backbone that were accessible to TFA at 1.5 and 23 °C. The fraction of accessible fluorophores was found to be equal to 0.5 in all experiments.

While this  $f_a$  value is relatively small for PIM-1 dissolved in DCM, reflecting the slow dynamics of the PIM-1 backbone, it was large for the insoluble PIM-1 membrane in hexane. Furthermore, the linear Stern–Volmer plots obtained for the quenching of PIM-1 in DCM and the PIM-1 membrane by TBA indicated that the constituting units of PIM-1 are fully accessible to the solvent or that  $f_a$  equaled 1.0. These results are most certainly a consequence of the high porosity exhibited by the PIM-1 matrix as it is being used to prepare microporous polymeric membranes.

The same values found for  $f_a$  for the experiments carried out also suggest that PIM-1 exhibits a conformation in solution that is similar to that adopted in the bulk. This conclusion reflects the inherent stiffness of the PIM-1 backbone that undergoes slow molecular rearrangements on the fast fluorescence time scale. The procedure established in this study to determine the accessibility of a polymer matrix to a quencher can be used to probe quantitatively the level of solvent accessibility of other PIM membranes as a function of the PIM molecular structure. High porosity of a given PIM membrane is expected to be matched by high accessibility, as determined by our fluorescence experiments. These experiments should be of interest to experimentalists involved in the characterization of the properties of PIM-based materials.

## ■ ASSOCIATED CONTENT

### ■ Supporting Information

Plot of the wavenumbers at the absorption and fluorescence maxima as a function of TFA volume fraction in DCM; fluorescence spectra acquired at 1.5 °C; fluorescence decays of PIM-1 in DCM acquired at different emission wavelengths; tables with characteristic photophysical properties of M-1 in different solvents; pre-exponential factors and decay times retrieved from the multiexponential fits of the fluorescence decays. This material is available free of charge via the Internet at <http://pubs.acs.org>.

## ■ AUTHOR INFORMATION

### Present Addresses

<sup>||</sup>EO Research Department, Petroleum Exploration & Production Research Institute, Sinopec, Beijing 100083, China.

<sup>⊥</sup>CIBA Vision GmbH, Bauhofstrasse 16, 63868 Grossostheim, Germany.

### Notes

The authors declare no competing financial interest.

## ■ ACKNOWLEDGMENTS

S.C., W.Y., and J.D. are thankful for NSERC and OGS financial support.

## ■ REFERENCES

- (1) Budd, M. P.; Ghanem, B. S.; Makhseed, S.; McKeown, N. B.; Msayib, K. J.; Tattershall, C. E. Polymers of Intrinsic Microporosity (PIMs): Robust, Solution-Processable, Organic Nanoporous Materials. *Chem. Commun.* **2004**, 230–231.
- (2) McKeown, N. B.; Budd, P. M.; Msayib, K. J.; Ghanem, B. S.; Kingston, H. J.; Tattershall, C. E.; Makhseed, S.; Reynolds, K. J.; Fritsch, D. Polymers of Intrinsic Microporosity (PIMs): Bridging the Void between Microporous and Polymeric Materials. *Chem.—Eur. J.* **2005**, *11*, 2610–2620.
- (3) Budd, P. M.; McKeown, N. B.; Fritsch, D. Free Volume and Intrinsic Microporosity in Polymers. *J. Mater. Chem.* **2005**, *15*, 1977–1986.
- (4) McKeown, N. B.; Budd, P. M. Polymers of Intrinsic Microporosity (PIMs): Organic Materials for Membrane Separations, Heterogeneous Catalysis and Hydrogen Storage. *Chem. Soc. Rev.* **2006**, *35*, 675–683.
- (5) Ghanem, B. S.; McKeown, N. B.; Budd, P. M.; Fritsch, D. Polymers of Intrinsic Microporosity Derived from Bis(phenazyl) Monomers. *Macromolecules* **2008**, *41*, 1640–1646.
- (6) Staiger, C. L.; Pas, S. J.; Hill, A. J.; Cornelius, C. J. Gas Separation, Free Volume Distribution, and Physical Aging of a Highly Microporous Spirobisindane Polymer. *Chem. Mater.* **2008**, *20*, 2606–2608.
- (7) Thomas, S.; Pinnau, I.; Du, N.; Guiver, M. D. Pure- and Mixed-Gas Permeation Properties of a Microporous Spirobisindane-Based Ladder Polym (PIM-1). *J. Membr. Sci.* **2009**, *333*, 125–131.
- (8) Thomas, S.; Pinnau, I.; Du, N.; Guiver, M. D. Hydrocarbon/Hydrogen Mixed-Gas Permeation Properties of PIM-1, an Amorphous Microporous Spirobisindane Polymer. *J. Membr. Sci.* **2009**, *338*, 1–4.
- (9) Fritsch, D.; Merten, P.; Heinrich, K.; Lazar, M.; Priske, M. High Performance Organic Solvent Nanofiltration Membranes: Development and Thorough Testing of Thin Film Composite Membranes Made of Polymers of Intrinsic Microporosity (PIMs). *J. Membr. Sci.* **2012**, *401–402*, 222–231.
- (10) McKeown, N. B.; Ghanem, B.; Msayib, K. J.; Budd, P. M.; Tattershall, C. E.; Mahmood, K.; Tan, S.; Book, D.; Langmi, H. W.; Walton, A. Towards Polymer-Based Hydrogen Storage Materials: Engineering Ultramicroporous Cavities within Polymers of Intrinsic Microporosity. *Angew. Chem., Int. Ed.* **2006**, *45*, 1804–1807.
- (11) Wang, Y.; McKeown, N. B.; Msayib, K. J.; Turnbull, G. A.; Samuel, I. D. W. Laser Chemosensor with Rapid Responsivity and Inherent Memory Based on a Polymer of Intrinsic Microporosity. *Sensors* **2011**, *11*, 2478–2487.
- (12) Rakow, N. A.; Wendland, M. S.; Trend, J. E.; Poirier, R. J.; Paolucci, D. M.; Maki, S. P.; Lyons, C. S.; Swierczek, M. J. Visual Indicator for Trace Organic Volatiles. *Langmuir* **2010**, *26*, 3767–3770.
- (13) Song, J.; Du, N.; Dai, Y.; Robertson, G. P.; Guiver, M. D.; Thomas, S.; Pinnau, I. Linear High Molecular Weight Ladder Polymers by Optimized Polycondensation of Tetrahydroxytetramethylspirobisindane and 1,4-Dicyanotetrafluorobenzene. *Macromolecules* **2008**, *41*, 7411–7417.
- (14) Zhang, Q.; Chen, G.; Zhang, S. Synthesis and Properties of Novel Soluble Polyimides Having a Spirobisindane-Linked Dianhydride Unit. *Polymer* **2007**, *48*, 2250–2256.
- (15) Ghanem, B. S.; McKeown, N. B.; Budd, P. M.; Fritsch, D. Polymers of Intrinsic Microporosity Derived from Bis(phenazyl) Monomers. *Macromolecules* **2008**, *41*, 1640–1646.
- (16) Ghanem, B. S.; McKeown, N. B.; Budd, P. M.; Al-Harbi, N. M.; Fritsch, D.; Heinrich, K.; Starannikova, L.; Tokarev, A.; Yampolskii, Y. Synthesis, Characterization, and Gas Permeation Properties of a Novel Group of Polymers with Intrinsic Microporosity: PIM-Polyimides. *Macromolecules* **2009**, *42*, 7881–7888.
- (17) Ghanem, B. S.; Hashem, M.; Harris, K. D. M.; Msayib, K. J.; Xu, M.; Budd, P. M.; Chaukura, N.; Book, D.; Tedds, S.; Walton, A.; McKeown, N. B. Triptycene-Based Polymers of Intrinsic Microporosity: Organic Materials That Can Be Tailored for Gas Adsorption. *Macromolecules* **2010**, *43*, 5287–5294.
- (18) Fritsch, D.; Bengtson, G.; Carta, M.; McKeown, N. B. Synthesis and Gas Permeation Properties of Spirobisindane-Based Polymers of Intrinsic Microporosity. *Macromol. Chem. Phys.* **2011**, *212*, 1137–1146.
- (19) Emmeler, T.; Heinrich, K.; Fritsch, D.; Budd, P. M.; Chaukura, N.; Ehlers, D.; Rätzke, K.; Faupel, F. Free Volume Investigation of Polymers of Intrinsic Microporosity (PIMs): PIM-1 and PIM1 Copolymers Incorporating Ethanoanthracene Units. *Macromolecules* **2010**, *43*, 6075–6084.
- (20) Weber, J.; Schmidt, J.; Thomas, A.; Böhlmann, W. Micropore Analysis of Polymer Networks by Gas Sorption and <sup>129</sup>Xe NMR Spectroscopy: Toward a Better Understanding of Intrinsic Microporosity. *Langmuir* **2010**, *26*, 15650–15656.
- (21) Shantarovich, V. P.; Suzuki, T.; Ito, Y.; Kondo, K.; Yu, R. S.; Budd, P. M.; Yampolskii, Y. P.; Berdonosov, S. S.; Eliseev, A. A.



Structural Heterogeneity in Glassy Polymeric Materials Revealed by Positron Annihilation and Other Supplementary Techniques. *Phys. Status Solidi C* **2007**, *4*, 3776–3779.

(22) Maffei, A. V.; Budd, P. M.; McKeown, N. B. Adsorption Studies of a Microporous Phthalocyanine Network Polymer. *Langmuir* **2006**, *22*, 4225–4229.

(23) Staiger, C. L.; Pas, S. J.; Hill, A. J.; Cornelius, C. J. Gas Separation, Free Volume Distribution, and Physical Aging of a Highly Microporous Spirobisindane Polymer. *Chem. Mater.* **2008**, *20*, 2606–2608.

(24) de Miranda, R. L.; Kruse, J.; Ratzke, K.; Faupel, F.; Fritsch, D.; Abetz, V.; Budd, P. M.; Selbie, J. D.; McKeown, N. B.; Ghanem, B. S. Unusual Temperature Dependence of the Positron Lifetime in a Polymer of Intrinsic Microporosity. *Phys. Status Solidi RRL* **2007**, *1*, 190–192.

(25) Lakowicz, J. R. *Principles of Fluorescence Spectroscopy*; Kluwer: New York, 1999; pp 248–249.

(26) Kricheldorf, H. R.; Lomadze, N.; Fritsch, D.; Schwarz, G. Cyclic and Telechelic Ladder Polymers Derived from Tetrahydroxytetramethylspirobisindane and 1,4-Dicyanotetrafluorobenzene. *J. Polym. Sci., Part A: Polym. Chem.* **2006**, *44*, 5344–5352.

(27) The model compound M-1 was made in a similar manner as PIM-1. A portion of 6 mmol of tert-butylcatechol was dissolved in dimethylformamide. Under a flow of argon, 3 mmol of 1,4-dicyanotetrafluorobenzene was added followed by 6.3 mmol of powdered, dry  $K_2CO_3$ . The solution was magnetically stirred and heated at 70 °C for 23 h. The yellow-green suspension was mixed into water. The precipitate was vacuum filtrated, washed with acetone, and dried in a vacuum (80% yield). MP 344–346 °C.  $^1H$  NMR ( $CDCl_3$ ): 1.29 (s, 18H), 6.91 (dd, 2H), 7.02 (s, 2H), 7.03 ppm (dd, 2H).

(28) Press, W. H.; Flannery, B. P.; Teukolsky, S. A.; Vetterling, W. T. *Numerical Recipes. The Art of Scientific Computing (Fortran Version)*; Cambridge University Press: Cambridge, U.K., 1992.

(29) *CRC Handbook of Chemistry and Physics*; Lide, D. R., Ed.; CRC Press: Boca Raton, FL, 2005.

(30) Masuhara, H.; Hino, T.; Mataga, N. Ionic Photodissociation of Excited Electron Donor-Acceptor Systems. I. An Empirical Equation on the Relationship between the Yield and the Solvent Dielectric Constant. *J. Phys. Chem.* **1975**, *79*, 994–1000.

(31) Ghosh, H. N.; Pal, H.; Sapre, A. V.; Mittal, J. P. Charge Recombination Reactions in Photoexcited Fullerene C<sub>60</sub>-Amine Complexes Studied by Picosecond Pump Probe Spectroscopy. *J. Am. Chem. Soc.* **1993**, *115*, 11722–11727.

(32) Rath, M. C.; Pal, H.; Mukherjee, T. Interactions of Ground and Excited ( $S_1$ ) States of C<sub>60</sub> and C<sub>70</sub> with Aromatic Amines: Exciplex and Charge-Transfer Emissions. *J. Phys. Chem. A* **1999**, *103*, 4993–5002.

(33) Brand, L.; Seliskar, C. J.; Turner, D. C. In *Probes of Structure and Function of Macromolecules and Membranes*; Chance, B., Blaisie, J.-K., Eds.; Academic Press: New York, 1971; pp 17–39.

(34) Fung, S.-Y.; Duhamel, J.; Chen, P. Solvent Effect on the Photophysical Properties of the Anticancer Agent Ellipticine. *J. Phys. Chem. A* **2006**, *110*, 11446–11454.

(35) Siu, H.; Duhamel, J. Associations between a Pyrene-Labeled Hydrophobically Modified Alkali Swellable Emulsion Copolymer and Sodium Dodecyl Sulfate Probed by Fluorescence, Surface Tension, and Rheology. *Macromolecules* **2006**, *39*, 1144–1155.

(36) Heuchel, M.; Fritsch, D.; Budd, P. M.; McKeown, N. B.; Hofmann, D. Atomistic Packing Model and Free Volume Distribution of a Polymer with Intrinsic Microporosity (PIM-1). *J. Membr. Sci.* **2008**, *318*, 84–99.

(37) Winnik, M. A.; Bystryak, S. M.; Liu, Z.; Siddiqui, J. Synthesis and Characterization of Pyrene-Labeled Poly(ethyleneimine). *Macromolecules* **1998**, *31*, 6855–6864.

(38) Claracq, J.; Santos, S. F. C. R.; Duhamel, J.; Dumousseaux, C.; Corpart, J.-M. Probing the Viscous Interior of Styrene/Maleic Anhydride Copolymer Aggregates in Water by Fluorescence Spectroscopy. *Langmuir* **2002**, *18*, 3829–3835.

(39) Siddique, B.; Duhamel, J. Effect of Polypeptide Sequence on Polypeptide Self-Assembly. *Langmuir* **2011**, *27*, 6639–6650.